JOURNAL OF GEOPHYSICAL RESEARCH, VOL. 104, NO. D2, PAGES 1973–1990, JANUARY 27, 1999

# Simulated time-dependent climate response to solar radiative forcing since 1600

D. Rind, J. Lean,[1] and R. Healy[2]

Goddard Space Flight Center, Institute for Space Studies, New York

**Abstract.** Estimated solar irradiance variations since 1500 have been used to force the GISS atmospheric GCM coupled to a mixed layer "$q$-flux" ocean with heat diffusion through the bottom of the mixed layer. The goal is to assess solar-induced climate change in preindustrial and postindustrial epochs. Six simulations and control runs were made to test the effects of different initial conditions, estimates of initial solar forcing conditions, and ocean heat uptake. The results show that an estimated solar forcing increase of 0.25% accounts for a 0.45°C temperature increase since 1600 and an increase of about 0.2°C over the past 100 years. Global surface temperatures lag solar fluctuations by up to 10 years; the lag is greater over the oceans and so is the correlation due to reduced noise. With only a mixed layer ocean the phase lag is 5 years less. Solar forcing and water vapor feedback each directly account for 35% of the temperature response, with cloud cover changes contributing 20% and sea ice/snow cover 10%. Uncertainty in the initial radiation imbalance or solar forcing affects the surface temperatures for 60–90 years. Modeled and observed periodicities show dominance of long-period forcing (>50 years), as provided by the solar input in these experiments. Tropical temperatures correlate best with solar forcing, due to the influence of water vapor feedback, especially at these multidecadal periods. Sea ice and extratropical temperatures have less long-period power, while high-frequency fluctuations dominate simulated cloud cover variations, which are relatively independent of solar forcing changes. Global and extratropical precipitation increase as the climate warms, but not low and subtropical precipitation, due to conflicting influences of absolute temperature and temperature gradient changes. Solar forcing by itself was not sufficient to produce the rapid warming during the last several decades. A comparison experiment varying trace gas forcing suggests that if the solar estimate is correct, then negative forcing by tropospheric aerosols (and perhaps volcanoes, ozone, and land use changes) has been about $-1.2$ W m$^{-2}$ since 1700, implying approximately equal contribution from direct and indirect tropospheric aerosol effects.

## 1. Introduction

There has been much debate about the potential influence of solar forcing relative to trace gas forcing of climate change during the past century and, in fact, extending back for a millennium. Was the general cooling, referred to as the "Little Ice Age," the result of solar-induced climate change, and how much of recent global warming signifies recovery from that cool epoch? The answers to these questions have future climate implications, for they would indicate what climate sensitivity to expect from future trace gas or solar variations. They also relate to questions of what solar irradiance variations can be expected. Paleoclimate studies indicate that the Little Ice Age may be the latest manifestation of a 1500 year climate oscillation present throughout the Holocene [*Bond et al*., 1998]. If the Maunder Minimum sunspot disappearance, which coincides well with the Little Ice Age time period [*Eddy*, 1976], caused the Little Ice Age, it might therefore be responsible for the Holocene oscillations, implying a similar periodicity in solar irradiance reductions.

Several previous modeling studies have addressed the influence of solar variability on climate in the recent past. Using functional relationships between assumed solar forcing and surface temperature response, both *Kelly and Wigley* [1992] and *Schlesinger and Ramankutty* [1992] suggested a partial solar influence. *Rind and Overpeck* [1994] using the Goddard Institute for Space Studies (GISS) general circulation model (GCM) investigated the equilibrium response to a solar irradiance variation of $-0.25\%$ (as ascribed by *Lean et al*. [1992] to the Maunder Minimum); their results showed a global cooling of 0.45°C. *Cubasch et al*. [1997] used a coupled atmosphere-ocean model to investigate the response to a prescribed solar variation, producing an overall response since the Maunder Minimum of about 0.5°C for an irradiance change of 0.35% [*Hoyt and Schatten*, 1993].

In this paper, we describe experiments which were performed by inputting prescribed variations in solar irradiance to the GISS GCM and calculating the time-dependent climate model response from the Maunder Minimum (commencing in either 1500 or 1600) to the present. "Proving" the influence of the Sun on climate requires that the input solar forcing be correct, the GCMs have the proper sensitivity, and the oceans absorb the proper amount of heat to provide an accurate rate

[1]E. O. Hulbert Center for Space Research, Naval Research Laboratory, Washington, D. C.

[2]Center for Climate Systems Research, Columbia University, New York.



Paper number 1998JD200020.
0148-0227/99/1998JD200020$09.00

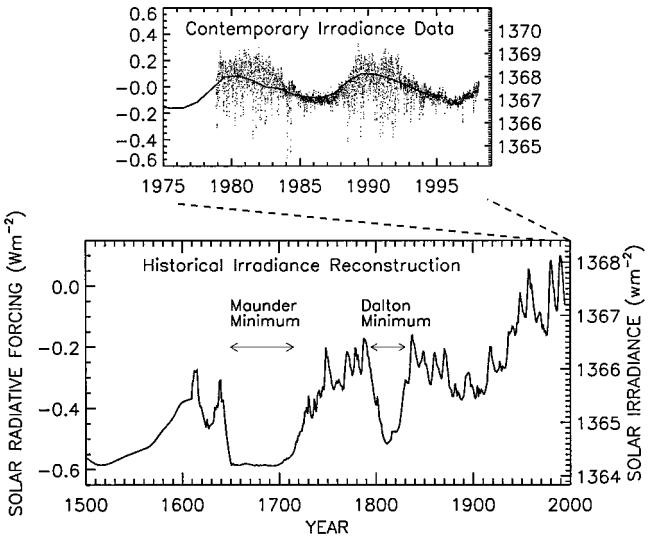


**Figure 1.** (top) Historical annual irradiance reconstruction (solid line) used to force the GISS GCM in these experiments. Also shown is a comparison with a composite record of daily measured solar total irradiance (symbols) [from *Frohlich and Lean*, 1998]. (bottom) The reconstructed annual irradiance since 1500. Four of the six model simulations commenced in 1615 and two in 1500. The solar radiative forcing axis (shown on the left-hand ordinate) is derived from the measured irradiance at the top of the Earth's atmosphere (shown on the right-hand ordinate) by adjusting for Earth's albedo and geometry ($\times 0.7/4$). Identified (bottom) are two epochs of anomolously low solar activity, termed the Maunder and Dalton minima.

of climate change. Yet because of their current uncertainties, none of these components is known with the required degree of accuracy. Our adopted solar forcing estimates derive from recent satellite observations and historical recordings, as well as stellar intensity fluctuations. Long-term changes depend upon an assumed variation in background network radiation of the Sun that correlates with solar (sunspot group) activity levels [*Hoyt et al*., 1994] and which tracks $^{14}$C and $^{10}$Be variations [*Lean et al*., 1995]. The GISS GCM sensitivity, of $\sim$1 W m$^{-2}$ is at the high end of the *Intergovernmental Panel on Climate Change* (*IPCC*) [1996] estimated range of possible sensitivities, although it is similar to many other GCM values. While the heat uptake by the ocean, parameterized as vertical heat diffusion through the bottom of the mixed layer, matches observations of tracer distribution in the ocean [*Hansen et al*., 1984], true ocean mixing of heat to depth is not produced in this manner. Thus these experiments are an exploration, rather than a specification of the role of solar irradiance variations in the climate variations of the past half millennium, to be subsequently improved as the various components of the problem become better defined.

## 2. Method and Experiments

An evaluation of the possible influence of solar irradiance variations on the climate system requires an estimate of changes in solar radiative forcing with time. We use the estimates of historical total irradiance variations since 1600 reconstructed by *Lean et al*. [1995] and extend them back to 1500 by using scaled $^{14}$C and $^{10}$Be variations. The solar forcing, shown in Figure 1, corresponds to a 0.25% irradiance increase from the Maunder Minimum to the present. We note that the variations are somewhat smaller than estimated by some other reconstructions, whose change since the Maunder Minimum is in the range of 0.35% [*Hoyt and Schatten*, 1993] to 0.65% [*Reid*, 1997]. At this time, it is not possible to confidently distinguish which values are more accurate, although all have similar patterns.

Solar forcing, so defined, was input to the GISS coarse resolution ($8^\circ \times 10^\circ$) GCM [*Hansen et al*., 1983]; while a newer version of the GCM exists with finer horizontal resolution, the coarse grid version permitted a number of long (400 and 500 years) experiment runs to be conducted within a realistic time frame. As the newer model has a slightly reduced sensitivity ($\sim$0.85°C per W m$^{-2}$), its simulated climate response would probably be slightly smaller as well. To separate the solar forcing response from ocean heat transport change (e.g., North Atlantic Deep Water variation), another potential mechanism for influencing the Little Ice Age climate [*Rind and Overpeck*, 1994], and to avoid model "climatic drift", we use the version of the ocean model with specified heat transports ($Q$ fluxes) and heat diffusion through the bottom of the variable depth mixed layer [*Hansen et al*., 1988]. Note that this "no surprise" ocean does not incite the spatial structure associated with events such as El Niños; considering this limitation, and the model's coarse grid, we concentrate on the global and latitudinal average results. Any possible solar forcing effect on ocean circulation changes cannot be examined in these simulations.

Table 1 lists the individual experiments performed. Three simulations and control runs were made from 1610 to the present. In the subsequent discussion, these runs are referred to as the "standard simulations." Each control run started with the same atmospheric initial conditions as the companion experiment and ran for a similar length of time but with the solar irradiance kept at current-day values. A fourth run, from 1500 to the present, estimated the effect of pre-1600 forcing on the 17th century simulation. A fifth experiment delayed the variable solar forcing for 120 years to estimate the effect of uncertainties in the early solar reconstruction. In the last experiment, no heat diffusion was permitted through the bottom of the mixed layer to assess the impact of ocean-mixing uncertainties.

## 3. Results

### 3.1. Standard Simulations

Figure 2 shows the global, annual average surface air temperature changes as a function of time simulated by the three standard experiments; all results given are the differences between the simulation and a corresponding control run with no solar irradiance variation. In this and other figures we show the

**Table 1.** GCM Simulations of the Effect of Solar Forcing

| Experiment | Description |
|---|---|
| 1 | 1610–1995 with variable solar forcing |
| 2 | as experiment 1, started 6 months earlier |
| 3 | as experiment 1, randomly different initial conditions |
| 4 | 1500–1995 with variable solar forcing |
| 5 | current solar irradiance 1610–1730; then variable as in experiments 1–3 |
| 6 | as experiment 5 but no heat diffusion through bottom of the mixed layer |

Each experiment has a separate control run of equal duration. Experiments 1–3 constitute the standard runs.

individual years to emphasize the degree of interannual variability; subsequent figures will also include smoothing with a Stineman function covering ±10% of the data length. To minimize the sharp changes associated with the sudden introduction of reduced solar forcing, the standard experiment results are shown only from 1640 onward. Table 2a lists the correlations of these three simulations and of the average surface air temperature with the solar variations shown in Figure 1. The global average temperatures from the control run indicate that the individual years are independent, as their autocorrelation drops below 0.5 with a 1 year lag. Therefore for this number of data points, correlations of 0.1 are significant at the 5% level, and using the $Z$ test, so are differences in correlation coefficients of 0.04.

The correlation of the three-run average with solar irradiance has a peak value of 0.74 at a lag of 10 years. Thus solar forcing accounts for about 50% of the variance in the model-averaged simulation, with model variability accounting for the other 50%. Correlations of individual runs peak in the range 0.5 to 0.75, accounting for about 33% of the variance with solar forcing. The relatively large variation among individual runs necessitates multiple simulations as a prelude for reliable conclusions. As will be shown later, the correlation value is reduced somewhat due to the assumption of climate equilibrium at 1610. Although the average correlation is numerically highest with a 10 year lag (see Table 2a), a broad peak exists between 0 and 20 year lags with a little significant difference.

Implicit in the specified solar forcing are certain periodicities. These are shown explicitly in Figure 3 (top). While some power exists in the 11 and 22 years, most of the power in the reconstructed total irradiance occurs at longer periods. The variable nature of solar irradiance results in a nonstationary periodogram. The variation of forcing with time can be shown by demodulating the time series. This approach, like wavelet analysis or other nonstationary analysis techniques, characterizes the time dependence of local power over a range of specified periods for the duration of the time series [*Bloomfield*, 1976]. The demodulated amplitudes of the solar forcing are shown in Figure 4 (top). Forcing in the intermediate 50–80 year period peaks shortly after 1800 (as can also be seen in Figure 1). Decadal-scale and bidecadal scale forcing are absent during the Maunder Minimum, weak in the Dalton Minimum (1800–1830), and fairly regular since about 1840.

To illustrate the periodicities of the model's global temperature response, four periodograms were constructed using the four solar runs (experiments 1–4), then averaged; the resultant periodogram is shown in Figure 3 (middle). Although the signals shown are not detrended, a linear detrending produced little difference in the periodograms at these periods. With the four experiments and control runs, a $t$-test was utilized to

**Table 2a.** Correlations Between Solar Irradiance and Surface Temperature Responses in Standard Experiments

| | Lag, years | | | | | | |
|---|---|---|---|---|---|---|---|
| | 0 | 5 | 10 | 15 | 20 | 25 | 30 |
| Experiment 1 | 0.753 | 0.751 | 0.729 | 0.679 | 0.648 | 0.593 | 0.546 |
| Experiment 2 | 0.407 | 0.468 | 0.513 | 0.537 | 0.567 | 0.554 | 0.549 |
| Experiment 3 | 0.483 | 0.614 | 0.629 | 0.633 | 0.614 | 0.635 | 0.620 |
| Average (experiments 1–3) | 0.704 | 0.739 | 0.744 | 0.722 | 0.709 | 0.685 | 0.652 |

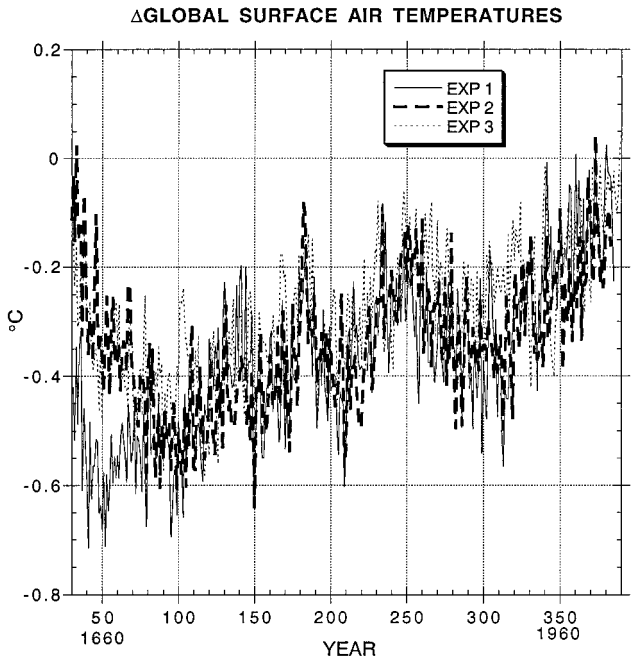


**Figure 2.** Global, annual average surface air temperature changes in the standard three experiments, which differ only in their initial atmospheric conditions. In all the figures, differences shown are between the experiment and a corresponding control run with no solar irradiance change.

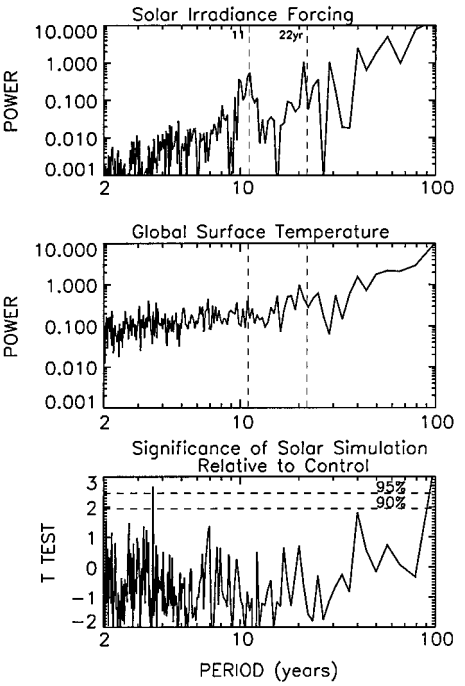


**Figure 3.** Periodograms of (top) the solar forcing time series, and (middle) the annually averaged surface air temperature response of the GCM, determined as the average of four periodograms from experiments 1–4. Calculations as in the work of *Horne and Baliunas* [1986]. (bottom) The student $t$-test of the difference between the average periodogram of the solar-forced simulation and the average periodogram of the four corresponding control runs (made without solar forcing).

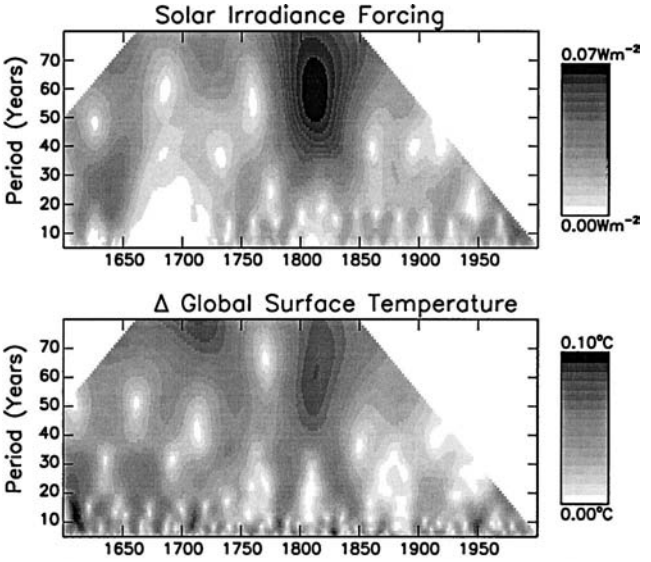


**Figure 4a.** Complex demodulation [*Bloomfield*, 1976] of the solar forcing and global annually averaged surface air temperature differences (of four experiments) characterizing the evolution of their local power, for periods from 5 to 80 years. The amplitudes of the periods present in the time series are shown in units of the time series and correspond to half the peak-to-peak range. (top) Solar forcing and (bottom) global annual average surface air temperature differences due to solar forcing.

determine significant differences associated with the solar forcing; most of the model's response is not significant (Figure 3 bottom). A demodulation of the global temperature change between the solar forcing runs and the control runs (Figure 4a, bottom) emphasizes that as in the case of the solar response, the global temperatures have nonstationary frequency/power relationship. Clearly, the power between 50 and 80 years in the solar forcing is evident in the model's response, peaking in the same years. Overall, the solar-global temperature correlation for periods in the range 0–80 years is 0.69, similar to that shown in Tables 2a and 2b for the entire frequency range, which includes the more dominant longer periods.

How do these periodicities change with latitude? The demodulated temperature changes for equatorial latitudes (16°N–16°S), midlatitudes (31°–63° latitude in both hemispheres), and the polar region (63° to the pole in both hemispheres) are presented in Figure 4b. The primary 50–80 year power is most prominent in the tropical region and diminishes toward higher latitude. Power at 20 years or less is evident at all latitudes, even during the Maunder Minimum when it is absent from the solar forcing (Figure 4a). Intermediate power (20–50 years) is much weaker at high latitudes. Overall, in this period range, solar forcing correlates with equatorial temperatures at 0.7, midlatitude temperatures at about 0.5, and high-latitude temperatures about 0.2.

**Table 2b.** Correlations Between Solar Irradiance and Surface Temperature Responses in Sensitivity Experiments

| | Lag, years | | | | | | |
|---|---|---|---|---|---|---|---|
| | 0 | 5 | 10 | 15 | 20 | 25 | 30 |
| | | | *Experiment 4* | | | | |
| Global | 0.799 | 0.799 | 0.780 | 0.722 | 0.668 | 0.625 | 0.594 |
| Land | 0.673 | 0.683 | 0.647 | 0.615 | 0.563 | 0.539 | 0.514 |
| Ocean | 0.813 | 0.816 | 0.806 | 0.795 | 0.727 | 0.671 | 0.626 |
| | | | *Experiment 6* | | | | |
| Global | 0.805 | 0.802 | 0.780 | 0.733 | 0.687 | 0.630 | 0.596 |
| Land | 0.686 | 0.649 | 0.612 | 0.565 | 0.522 | 0.495 | 0.452 |
| Ocean | 0.823 | 0.825 | 0.806 | 0.757 | 0.713 | 0.652 | 0.610 |

### 3.2. Feedbacks

In the model simulations, well-known feedbacks amplify the temperature response, including changes in water vapor, sea ice, and cloud cover. As shown in Figure 5 (top), water vapor varies with the global temperature response, being generally less in the colder years. Some differences exist among the simulations, with experiment 1 generally having slightly more water vapor. For the composite runs, the correlation between surface air temperature and water vapor change peaks at 0.92, with the highest value occurring with zero lag (Table 3). Water vapor changes are of the order of 2% of control run values.

Sea ice coverage shown in Figure 5 (middle) is, as expected, increased in the generally colder climate. Again, the various runs have some differences, with sea ice being somewhat less in experiment 1. For the composite runs, the correlation between surface air temperature and sea ice changes peaks at −0.57, again highest with zero lag. Sea ice changes are of the order of 4% of control run values.

Total cloud cover variations in the three runs are also shown in Figure 5 (bottom). The variation is such that cloud cover is less when temperatures are colder, because as climate cools,

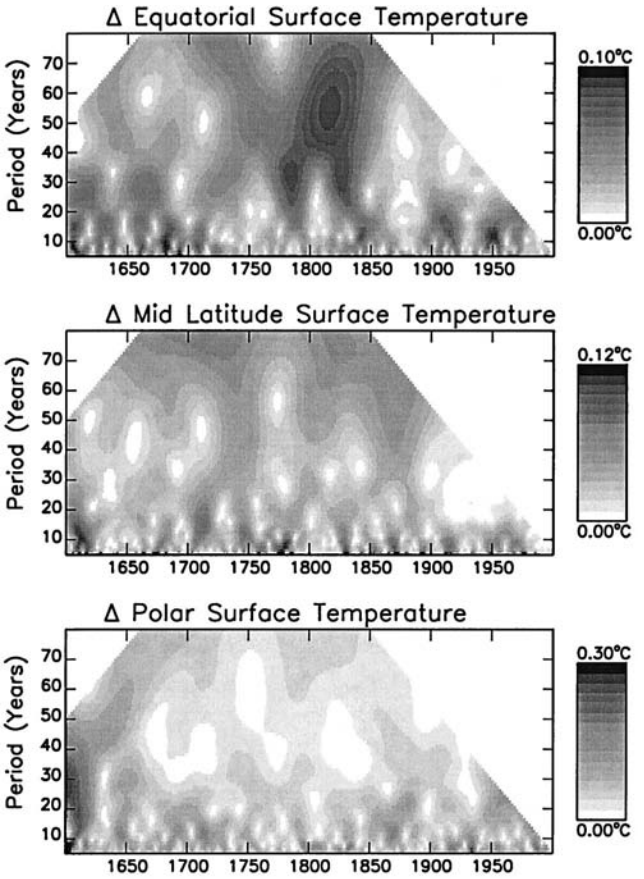


**Figure 4b.** As in Figure 4a surface temperature changes in the tropics (16°N–16°S) (top), at midlatitudes (31°–63° latitude) (middle) and in polar regions (63° to the pole) (bottom).

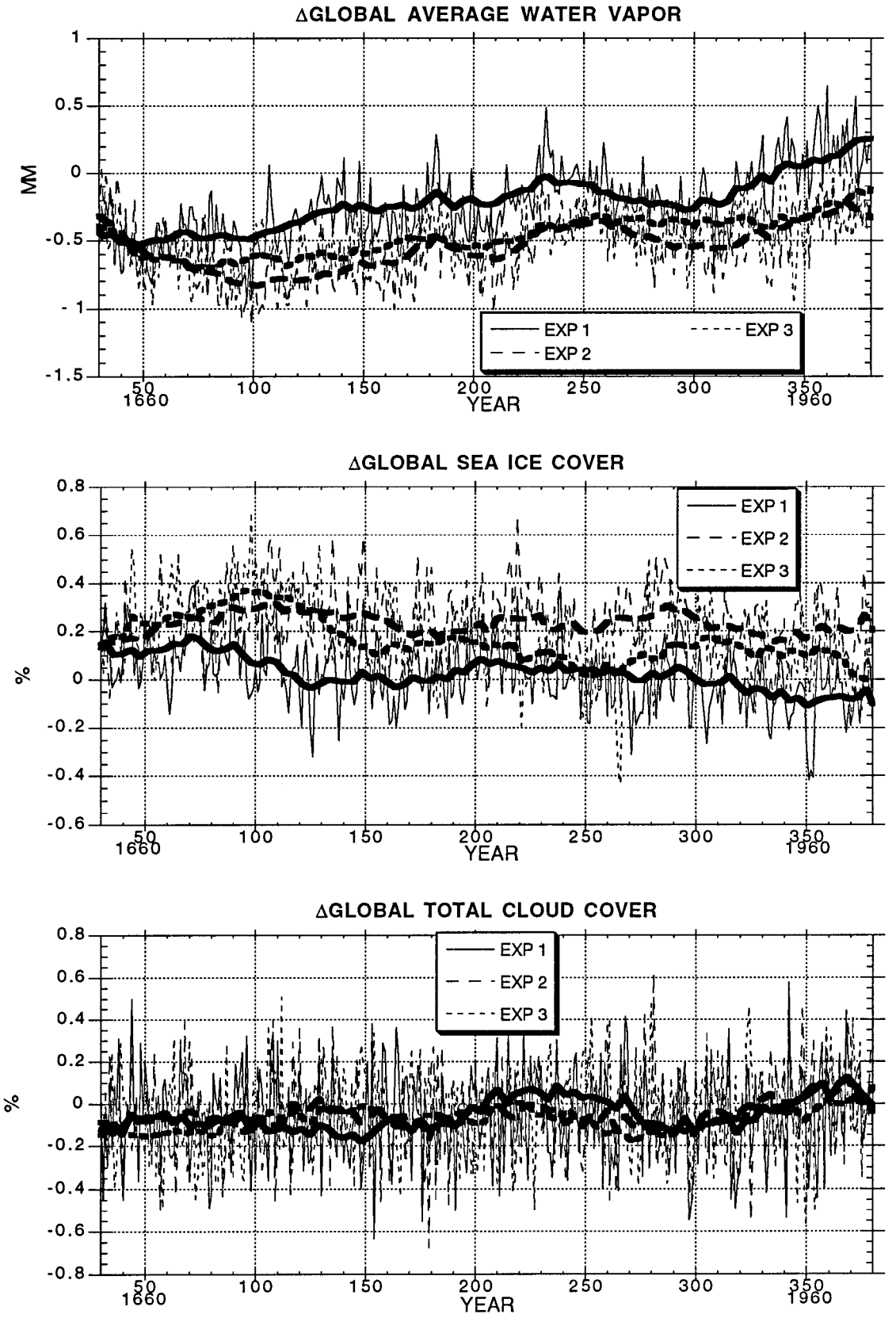


**Figure 5.** As in Figure 2 except for water vapor (top), sea ice cover (middle), and total cloud cover (bottom). In addition to the yearly results from the individual experiments, a smoothed curve is shown for each, constructed with a Stineman function applied to ±10% of the data range.

**Table 3.** Correlations Between Surface Air Temperature Changes and Feedbacks

| | Lag, years | | | | | |
|---|---|---|---|---|---|---|
| | −10 | −5 | 0 | 5 | 10 | 15 |
| Water vapor | 0.602 | 0.689 | 0.926 | 0.717 | 0.638 | 0.609 |
| Sea ice | −0.401 | −0.424 | −0.572 | −0.464 | 0.467 | 0.417 |
| Clouds | 0.141 | 0.063 | 0.162 | 0.175 | 0.082 | 0.074 |

high clouds decrease more than low clouds increase. This conclusion differs from that found in doubled $CO_2$ experiments with the GISS model [e.g., *Rind*, 1986], possibly because in these simulations the temperature changes are of reduced magnitude compared to those from doubled $CO_2$. The correlation of cloud cover with surface temperature is highest at 0–5 years lag, a distinctly different result from the water vapor correlation, due to the conflicting responses of high and low clouds.

As defined by *Hansen et al*. [1984], the "gain factor" is the ratio of the particular feedback portion of the temperature change to the total temperature change. *Hansen et al*. [1984] published the gain factors for solar irradiance forcing in the GISS model; the factors were calculated by using the three-dimensional (3-D) model responses to solar forcing in a 1-D radiative convective model. The globally averaged GCM changes in the various feedbacks were inserted individually into the 1-D model, and the surface air temperature change calculated from each effect. The gain factor for water vapor was 0.37, for sea ice 0.09, and for cloud cover 0.20. Using those results, we estimate the contribution of the various forcings/feedbacks to the overall temperature change from 1700 to the present (of ~0.45°C) as follows: direct solar change, 0.16°C; water vapor change, 0.16°C; cloud cover, 0.09°C; and sea ice, 0.04°C. This analysis assumes linear responses; as emphasized by *Rind et al*. [1995] for the total sea ice impact, nonlinear feedback among the different components means that limiting any one of them would impact all the others.

The different feedbacks also display different periods of response, as shown in the variations of the demodulated amplitudes with time in Figure 6. The water vapor response (Figure 6, top) shows substantial long-period energy (50–80 years), similar to that displayed by the equatorial temperatures (Figure 4b). The correlation over this frequency range between these two variables is 0.93, while global water vapor correlation drops when considering midlatitude temperatures (~0.6), and even more for polar temperatures (~0.3). The peak power around 1820 mimics that of the solar forcing.

The sea ice has somewhat weaker power at these longer periods, which maximizes when the temperature is relatively low (~1680 and 1880), emphasizing the rather obvious result that sea ice feedback is more effective in colder times. It correlates well with extratropical surface temperatures (−0.6). Cloud cover has weaker power at all periods greater than about 20 years (Figure 6 middle, bottom) and correlates poorly with temperatures at all latitudes (e.g., Table 3).

### 3.3. Sensitivity Experiments

With the goal of testing various uncertainties in the standard runs, we performed three sensitivity experiments. The first sensitivity experiment investigated the uncertainty associated with the initial climatic conditions at the start of the experiment (1610), which was assumed to be in equilibrium. We extended the solar irradiance forcing back to 1500 (as shown in Figure 1 and described above) and ran the model from that time forward. Differences with the three standard experiments are shown in Figure 7. Using the large negative solar forcing (relative to the present) ascribed to the years between 1500 and 1600 results in the surface air temperature at 1610 being approximately 0.2°C colder than the "neutral start" used in the standard runs. Temperatures remain somewhat cooler for about the next 50 years and, subsequently, rejoin the standard ensemble variations. Correlations between the surface air temperature change and the solar irradiance from 1610 onward, shown in Table 2b, are significantly higher than for the standard experiments, because the model has had 100 years to adjust to solar irradiance deficiencies, and at 1610 has a low temperature analogous to the reduced solar irradiance of that time.

In the second sensitivity experiment, we tested uncertainties in the solar forcing for the Maunder Minimum, which depend upon assumed but, thus far, unobserved fluctuations in the Sun's background network radiation by assuming there was no solar irradiance change for the first 120 years. After reintroducing the solar variation, surface temperatures took about 80 more years to match the temperature variations of the ensemble, a longer time than the previous experiment probably because of the greater amplitude of the sea ice feedback in a cooling experiment [e.g., *Rind et al*., 1995]. Subsequently, the correlations resumed their relationship with solar forcing (and are thus not shown in Table 2b). Hence the results of the first

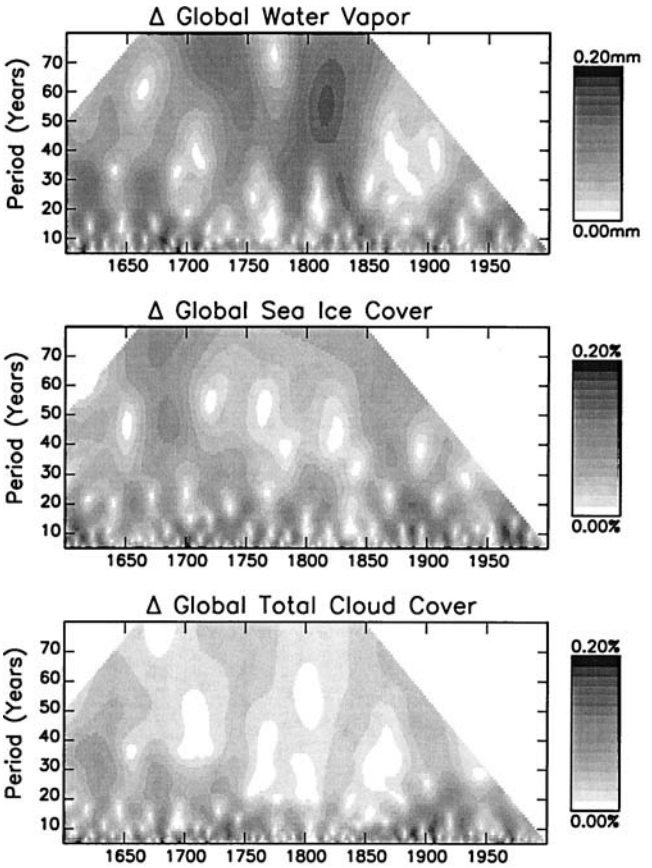


**Figure 6.** As in Figure 4 except for water vapor (top), sea ice cover (middle), and total cloud cover (bottom).

two sensitivity experiments suggest that the impact of the initial climate conditions, as forced by previous solar irradiance variations, lasts for some 60–80 years.

In the third sensitivity experiment, we investigated the uncertainty associated with ocean heat uptake by eliminating the heat diffusion through the bottom of the mixed layer. This permits the modeled climate system to respond to solar forcing entirely with a mixed layer heat capacity. As expected, this change amplified the climate response; for the sake of the simulation during the 1600s this experiment (and a corresponding control run with no heat diffusion through the bottom of the mixed layer) was also started in 1500. Cooling during the Maunder Minimum time period was much more extreme, reaching 1°C in certain years. The oscillations, in general, were larger; in this experiment, warming during the last century was of the order of 0.4°C, twice that produced in the standard ensemble runs. The correlation with solar forcing for the single simulation (Table 2b) is similar to the previous simulation from 1500, again larger than in the standard runs. The phase of the response now peaks at 0–10 years globally, or about 5 years earlier than with heat diffusion; therefore the heat diffusion to deeper layers (which, as noted by *Hansen et al*. [1984, 1988], was developed to provide a match with transient tracer observations such as tritium in the ocean) effectively adds a 5 year lag to the response. This lag is a complicated result of both the response to the initial forcing and the response time of the subsequent feedbacks.

The distribution of power as a function of period in the temperature response does not appear to depend upon the degree of diffusion through the base of the mixed layer, because a comparison of the two 500 year runs shows no significant differences.

### 3.4. Land/Ocean Response

We compare in Figure 8 the surface air temperature changes over land and ocean for the experiment begun in 1500. Fluctuations over land are larger, as expected, and show that relatively warm years can occur even during the years of general cooling associated with the Maunder Minimum. This is in agreement with observations showing the "Little Ice Age" to be typified by warm years among the general cooling [*Bradley and Jones*, 1992].

Table 2b lists the correlations with solar irradiance of land and ocean temperatures separately. Correlations are lower over land, as greater "noisiness" arises here, due to the land's smaller heat capacity. In contrast, the larger heat capacity of the ocean enhances slightly the correlation over the ocean relative to the global value. Surface air temperature changes

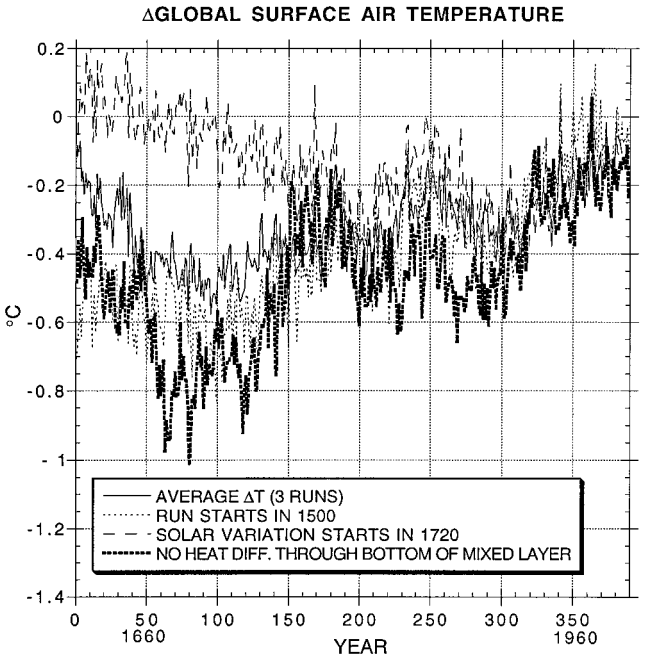


**Figure 7.** Comparison of surface air temperature changes between the standard experiments (average of experiments 1–3) and the sensitivity runs.

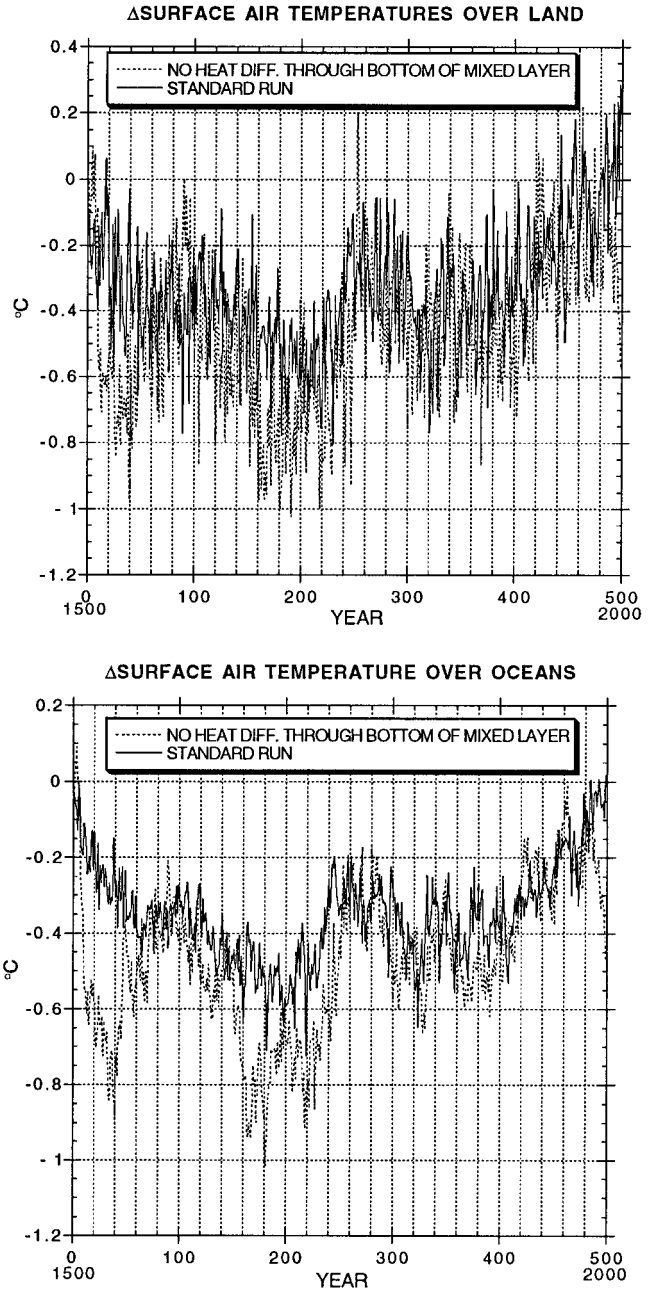


**Figure 8.** Surface air temperature changes over land (top) and ocean (bottom) for the experiment begun in 1500 (experiment 4) and the run with no heat diffusion through the bottom of the mixed layer (experiment 6).

over land peak with 0–10 year phase lag, while over the ocean, the peak is 0–15 years; the temperatures over land thus respond somewhat more rapidly. The land temperatures are affected by ocean temperature changes, and both are affected by the lag induced by the feedback amplification [*Hansen et al*., 1985].

For comparison, Figure 8 also shows the results for surface air temperature changes over land and ocean without heat diffusion through the bottom of the mixed layer, with corresponding correlations provided in Table 2b. As expected, lacking heat diffusion, the smaller effective ocean heat capacity increases the air temperature fluctuations over the ocean. This then augments the fluctuations in the temperatures of the air over land. As can be seen in Table 2b, the land response now peaks between 0 and 5 years and the ocean between 0 and 10 years. Both responses are 5 years faster than when the deeper ocean is involved, indicating again the dependence of the terrestrial air temperature change on ocean temperature changes and the amplifying feedbacks.

The periodogram for temperature changes over land does show somewhat more energy at decadal and shorter-period timescales with its smaller heat capacity, although the effects are still not significant (there is more noise as well).

### 3.5. Latitudinal Temperature Changes

How do the temperatures change as a function of latitude? This aspect of the model results is important in case solar forcing provides a particular latitudinal "footprint," allowing it to be differentiated from other potential climate perturbations. Changes in temperature at several latitudes are shown in Figure 9, for both experiments 2 and 3 (two of the three standard runs), to indicate the degree of consistency in different simulations. When compared with the global surface air temperature changes shown in Figure 2, overall, patterns are seen to be similar at the various latitudes, with significant correlations ranging from 0.65 to 0.18 between the global temperature and the individual latitudes shown. The correlations decrease with increasing latitude, at least partly because the lower latitude bands encompass more area and hence contribute more to the global mean temperature. The similarity in response between individual latitude bands also decreases with increasing latitude due to the greater noisiness in the extratropics and polar regions (note the change in scale in the figure). As noted above in conjunction with the discussion of Figure 4b, the equatorial temperatures and water vapor feedback have the most power at long periods, while extratropical temperatures and sea ice have somewhat less.

### 3.6. Latitudinal Temperature Gradients

Changes in the latitudinal temperature gradient are important because they affect various atmospheric dynamical features that influence climate. The Hadley cell circulation responds to changes in low-latitudinal temperature gradients, and midlatitude eddy energy responds to changes in midlatitude temperature gradients [e.g., *Rind*, 1998]. The general expectation is that these gradients should increase as climate cools, because high latitudes, affected by sea ice and snow feedbacks, should cool more than the tropics.

Illustrated in Figure 10a is the change in latitudinal temperature gradients for the 400 years of experiments 2 and 3; the same diagnostics are shown for the 500 year run and the run with no heat diffusion in Figure 10b. The mean changes are shown in parentheses. Since in all four experiments (numbers 2–4 and 6 in Table 1) the input solar irradiance was always less than current values (see Figure 1), the mean temperature change is negative. The low-latitudinal temperature gradient generally decreased slightly relative to the control run; as with reduced solar insolation, the tropics cooled more than lower midlatitudes; the change is of the order of 1%. At midlatitudes the gradient changes were small and of varying sign, with two simulations showing slight mean increases and two showing slight decreases. Overall, the mean hemispheric gradient, between low and high latitudes, increased in three of the four experiments, although again, the changes were small (of the order of 0.2%).

Linear regression between the global temperature changes and the change in gradient produces the statistics shown in Table 4. A negative value of the slope "$m$" indicates the latitudinal temperature gradient increases as temperature cools, or decreases as temperature warms. At low latitudes, $m$ is of both signs; the more significant positive correlations for the low-latitude gradient changes indicate the tropics warm more than lower middle latitudes as solar intensity increases. This would have the effect of increasing Hadley cell intensity. At midlatitudes, $m$ is generally negative and, again, generally significant, indicating the gradient decreased as climate warmed, which would decrease eddy energy. The gradient changes between the lowest and the highest latitudes are of different signs in different experiments (positive in the 400 year experiments, negative in the 500 year experiments) so do not indicate the expected high-latitude amplification in this hemisphere over the full course of these runs.

### 3.7. Precipitation Changes

Figure 11 shows the global temperature and precipitation changes for the two 500 year simulations. As indicated in Table 5, the two variables are well correlated, with temperature accounting for 25% and 50% of the global precipitation variance with and without heat diffusion through the bottom of the mixed layer. Significant changes occur more frequently without heat diffusion at the various latitudes, as the temperature responses themselves are larger (and from the Claussius-Clayperon relationship have an exponentially increasing impact on evaporation). At higher latitudes, precipitation increases as global temperatures rise, while at least with no heat diffusion, it decreases in the subtropics. Percentage-wise, the global precipitation changes are quite small, amounting to about 1–2% of the global mean value of 3 mm/d.

The precipitation changes at some individual latitudes are given in Figure 12 for these experiments. The broad peak-to-peak fluctuations are of the order of 10%. While there is much year-to-year variability independent of the global temperature trend, an out-of-phase relationship can be discerned at times between the tropics and the subtropics. For example, tropical precipitation is relatively high in the latter half of the 1500s, around 1700, and the latter half of the 1700s; these are all times with somewhat reduced precipitation at 27°N. An out-of-phase relationship might be expected here due to the influence of tropical precipitation changes on Hadley cell strength and subtropical subsidence. As indicated in Figure 10, the late 1700s was a time in the model of increased low-latitude temperature gradient, which would force an increase in Hadley cell intensity. However, subtropical and tropical precipitation also are affected by the global temperature changes independent of latitudinal gradient effects; for example, both show decreases in the mid-1600s when global temperatures cool. Therefore the

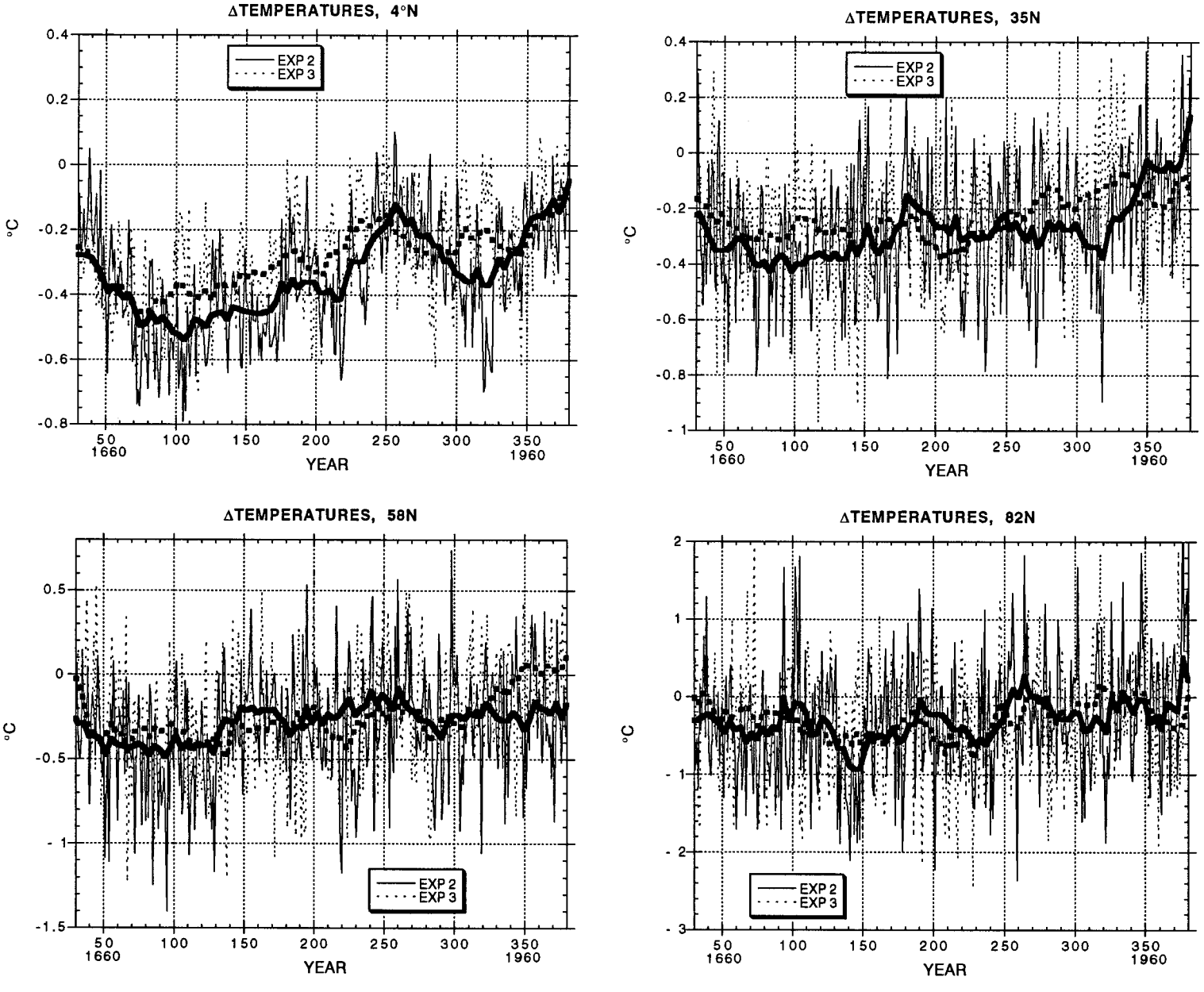


**Figure 9.** Annual surface air temperature changes at different latitudes in experiments 2 and 3. The smoothing approach is that used in Figure 5.

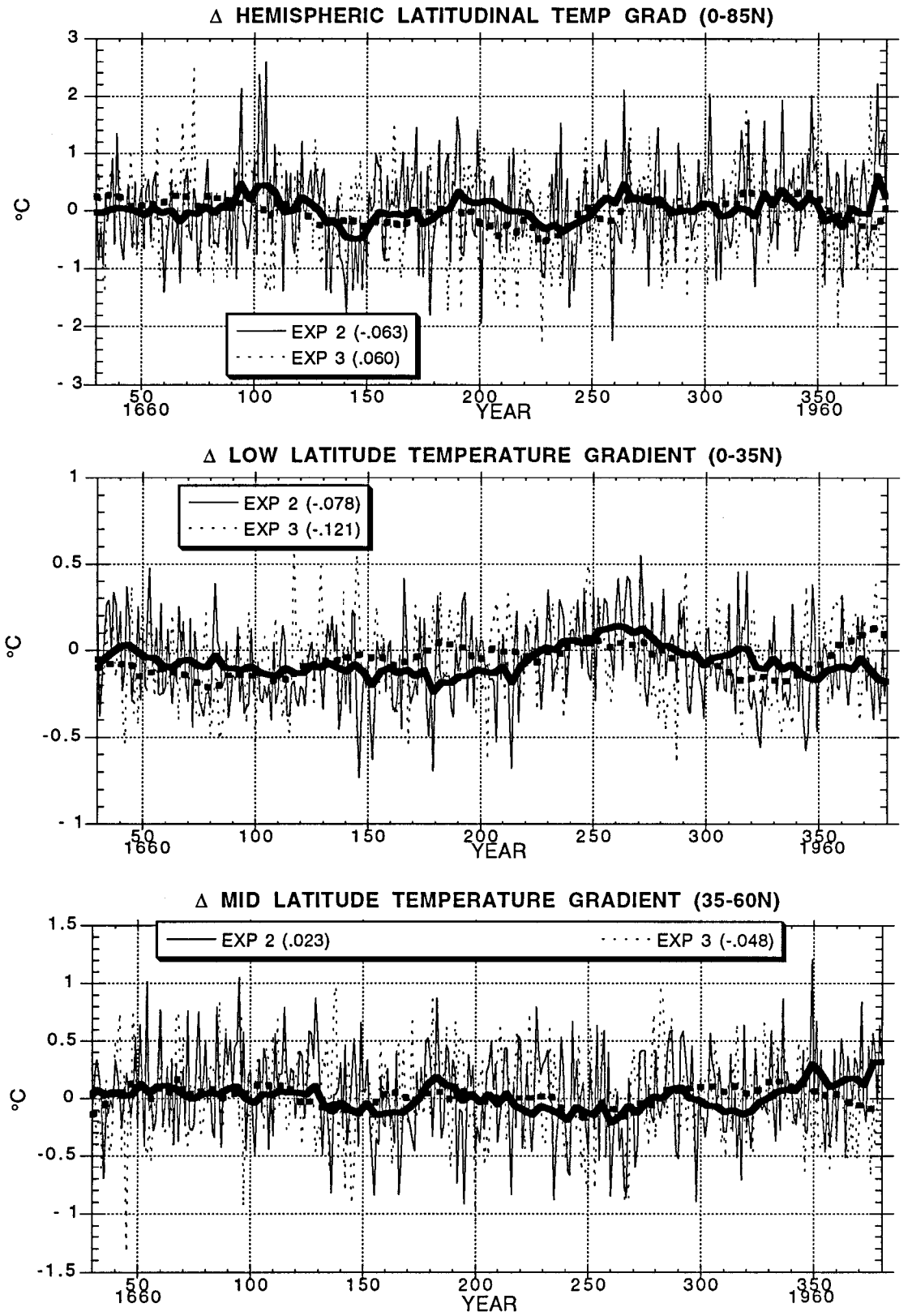


**Figure 10a.** Change in latitudinal surface air temperature gradients for experiments 2 and 3. The gradient is defined as a positive value, i.e., temperature at the lower latitude minus that at the higher latitude. Therefore a negative change indicates the lower-latitude temperature cooled more or warmed less than that of the higher latitude.

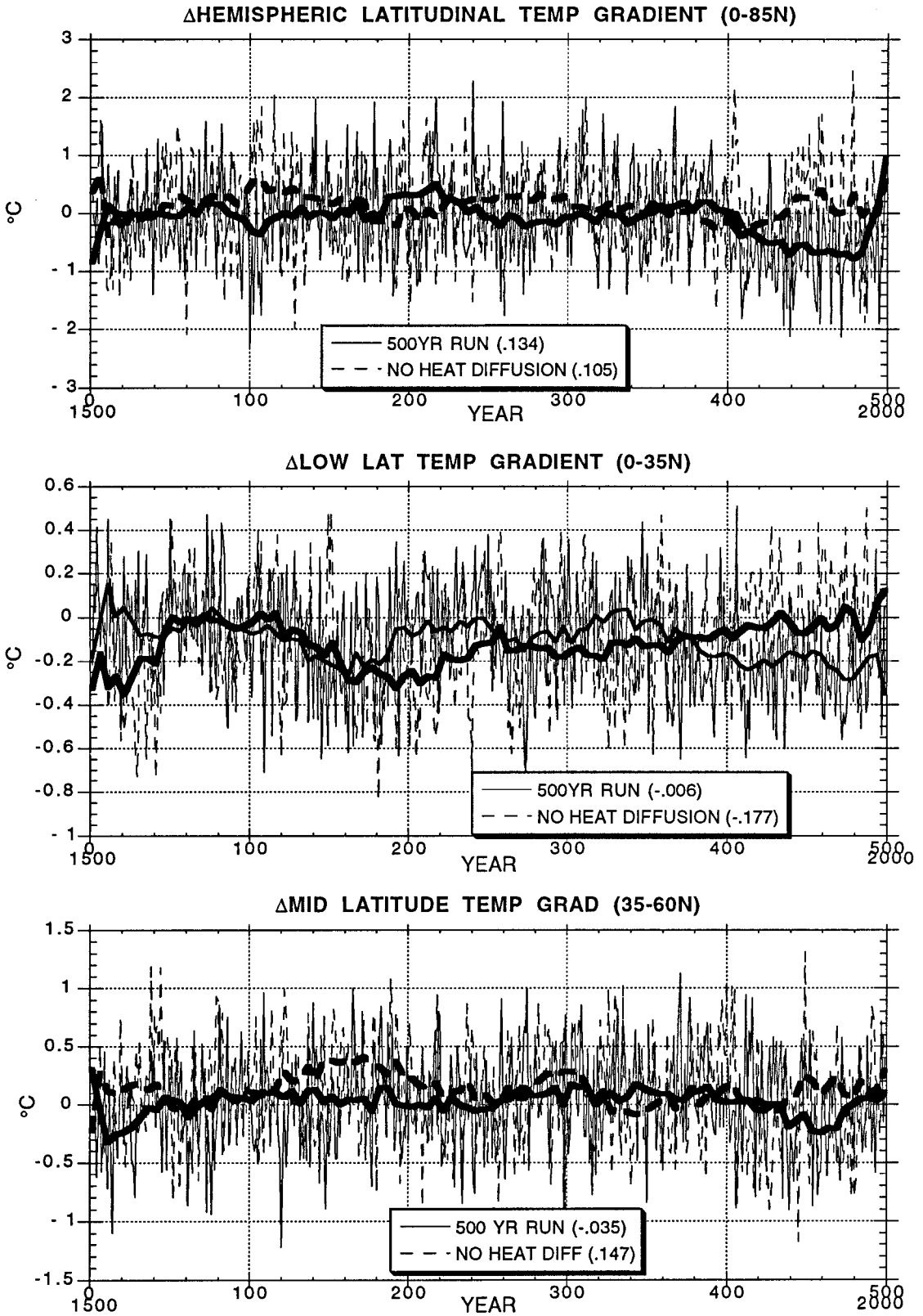


**Figure 10b.** As in Figure 7 except for experiments 4 and 6.

correlation between precipitation changes in the tropics and subtropics is not significant, in either run.

At middle latitudes it might be expected that as the latitudinal gradient increases, so does eddy energy and subsequent precipitation. Comparison of Figures 10b and 12 indicates a tendency for this effect: precipitation is largest in the early 1800s and late 1900s, when the gradient is slightly larger. In general, though, the increased temperature at middle latitudes

**Table 4.** Relationship Between Latitudinal Temperature Gradient Changes and Global Mean Temperature

| Experiment | Gradient | Linear Regression ($D$lat. temp. grad.) = $m$($D$global temp change) + $b$ | Correlation Coefficient |
|---|---|---|---|
| Experiment 1 | low latitude | $m = 0.24$, $b = 0$ | 0.14* |
| | midlatitude | $m = -0.03$, $b = -0.19$ | 0.07 |
| | hemispheric | $m = 0.15$, $b = 0.10$ | 0.03 |
| Experiment 2 | low latitude | $m = -0.17$, $b = -0.11$ | 0.11† |
| | midlatitude | $m = -0.51$, $b = -0.14$ | 0.19* |
| | hemispheric | $m = 0.88$, $b = 0.22$ | 0.16* |
| 500 years | low latitude | $m = -0.06$, $b = -1.23$ | 0.04 |
| | midlatitude | $m = -0.30$, $b = -0.08$ | 0.10† |
| | hemispheric | $m = -1.23$, $b = -0.55$ | 0.23* |
| No heat diffusion | low latitude | $m = 0.44$, $b = 0.11$ | 0.35* |
| | midlatitude | $m = -0.40$, $b = -0.12$ | 0.19* |
| | hemispheric | $m = -0.04$, $b = 0.07$ | 0.01 |

*Significant at 1% level.
†Significant at 5% level.

allows for more atmospheric water-holding capacity and greater precipitation capability, independent of any changes in eddy energy.

At higher latitudes the correlation of precipitation change with global temperature change is relatively high in both experiments, and the warming in the 20th century is clearly visible. Interestingly, the precipitation does not show a similar increase in the tropics or subtropics; the absolute magnitude of the 20th century temperature change is greater at the higher latitudes (see Figure 9 for the results from experiments 2 and 3), which amplifies the effect on precipitation.

## 4. Comparisons With Greenhouse Gas Forcing

Increases in greenhouse gases since the mid-18th century are also expected to produce a warming tendency over this same time frame. For comparison purposes, an additional simulation was run in which the solar irradiance was kept at current values, but greenhouse gases were allowed to increase in the observed manner (i.e., following the results from ice cores and measurements, as indicated in the various IPCC reports). Table 6 shows a comparison of the rates of warming produced by these difference forcing mechanisms in the model (solar results are from the standard ensemble runs). Also shown is the observed warming (courtesy of J. Hansen, available on the GISS home page, www.giss.nasa.gov). All values are given as differences for each 20 year period from the conditions prevailing in 1876–1895. We note that satellite retrievals, which have been thought to be at odds with surface-based estimates of recent warming, can be made consistent with the GISS records [*Prabhakara et al*., 1998].

The simulated trace gas warming is more than 3 times larger than the solar-induced warming, roughly consistent with the difference in radiative forcing since 1700 (approximately 0.6 W $m^{-2}$ for solar forcing and about 2.5 W $m^{-2}$ for the trace gas forcing). The observed warming is less than the trace-gas-induced warming by itself and only 50% of the sum of solar and trace gas warming. Of course, additional forcings were probably occurring during this time frame, particularly potential cooling associated with tropospheric aerosols. If one assumes the solar warming is correct, then only 0.257°C is left to be produced by the sum of trace gas and aerosol forcing over the past 100 years.

## 5. Discussion

The results of these transient experiments simulating climate response to solar forcing are generally consistent with the equilibrium response to a solar change of −0.25% [*Rind and Overpeck*, 1994], with a warming from the Maunder Minimum time period of slightly less than 0.5°C. This value is close to that reported by *Cubasch et al*. [1997], a similarity that is somewhat fortuitous. The GISS model has a sensitivity of close to 1°C per W $m^{-2}$, and the calculated change is in response to solar irradiance increase of 0.25% since 1650, after *Lean et al*. [1995]. The ECHAM 3 GCM, used by Cubasch et al. has a sensitivity that is ~35% lower than that of the GISS model, but the simulations adopted an overall solar irradiance change [from *Hoyt and Schatten*, 1993] about 20% higher.

The most provocative aspect of our results has to do with the postindustrial warming that occurs during the last 100 years. This warming is inherent in the estimated change in solar forcing which appears in all such reconstructions, including the empirical relationships derived by *Lean et al*. [1995], the functional relationships of *Schlesinger and Ramankutty* [1992] and *Kelley and Wigley* [1992], and the model results of *Cubasch et al*. [1997]. Most previous work concludes that the solar warming is not sufficient to account for the rapid warming during the last few decades, a result which is consistent with these experiments, and is emphasized in a companion paper (J. Lean et al., manuscript in preparation, 1998).

Over the longer time period, if the reconstructions by *Mann et al*. [1998] since 1600 are applicable (e.g., if their record can be inferred to indicate global temperature changes), the global temperature has warmed close to 1°C since 1700. Assuming the modeled solar warming of ~0.45°C is correct implies that the sum of trace gases and tropospheric aerosols (as well as any other effect, such as land albedo, volcanic aerosol, and ozone changes) would account for only ~0.55°C warming. The trace gas warming in the model since 1700 is about 1.4°C. Most of the other effects are likely of the order of a few tenths W $m^{-2}$ forcing and of opposing tendencies: land albedo increases, sporadic volcanic aerosols, and recent stratospheric ozone decreases produce cooling, while tropospheric ozone increases would provide warming. We therefore assume that tropospheric aerosols would have had to provide the required cooling of 0.85°C. For the simulation over that time the model has

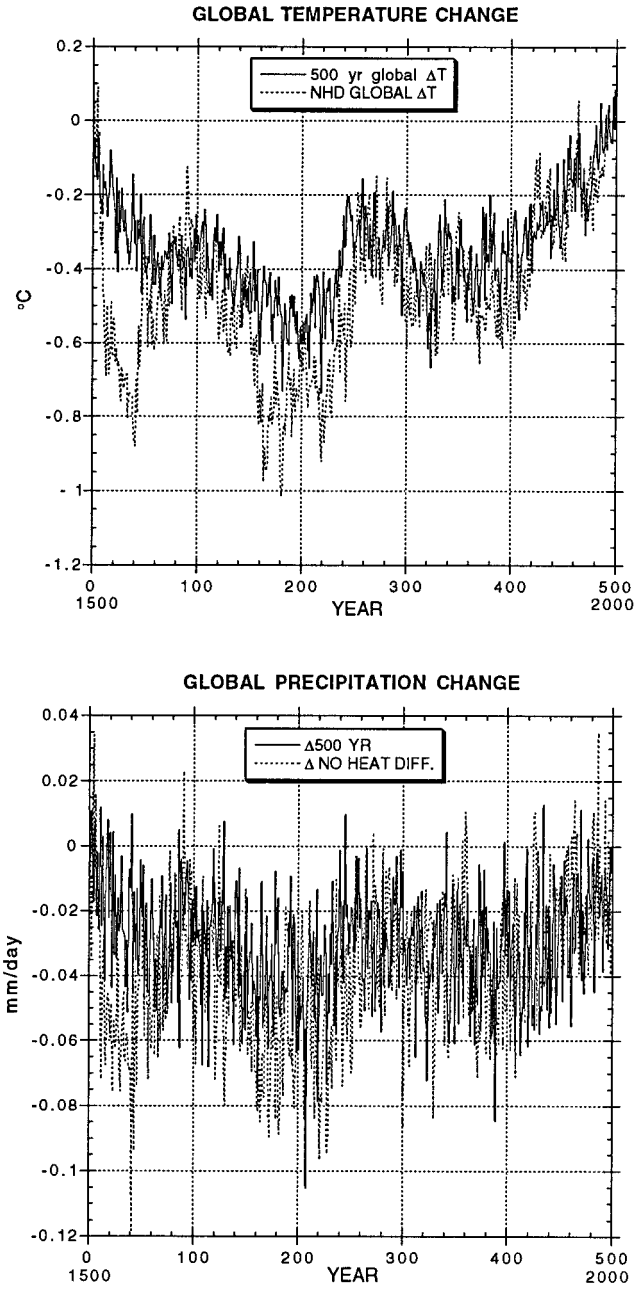


**Figure 11.** Global temperature and precipitation changes in experiments 4 and 6.

a climate sensitivity of about 0.7°C per W $m^{-2}$ (lower than its equilibrium value due to the unrealized warming associated with the ocean heat capacity); therefore the aerosol negative forcing since 1700 would have to have been $\sim -1.2$ W $m^{-2}$. As estimated by *IPCC* [1996], the direct effect of tropospheric aerosols should have been about $-0.5$ W $m^{-2}$, leaving an indirect effect (because of aerosol impacts on cloud cover) of $-0.7$ W $m^{-2}$, about midway within the range of (very uncertain) IPCC estimates.

Consistent with the previous studies, the solar forcing for the last two decades is insufficient to account for the recent global warming. The solar forcing over this time produces a warming of only 0.07°C (in Table 6, the warming in 1976–1995 minus 1876–1895 compared to that in 1956–1975 minus 1876–1895), while the observed warming of 0.25°C is much closer to that generated by trace gases alone (0.28°C). Of course, additional cooling mechanisms, such as tropospheric and volcanic aerosol changes and stratospheric ozone reductions, have also been occurring.

Temperature changes over the ocean are more highly correlated with solar irradiance variations than those over land. This contradicts the prevailing wisdom that the muting effects of the higher ocean heat capacity would make it easier to observe the changes over land. The lower heat capacity of the land surface leads to a noisier record of air temperatures, reducing coherent responses to forcing, which is of the same order as internal variability (as judged by the variability each produces in the model). Such a result complicates the detection issue, as most observations have historically been made over land.

The ocean response does have a greater time lag than the land, up to 5 years. This distinction does not depend on the degree of involvement of the deeper ocean, for it occurs both with and without heat diffusion through the bottom of the mixed layer. However, the system responds faster to solar forcing without such diffusion, a lag of 0–5 years compared to 0–10 years. Studies such as those of *White et al*. [1997], when applied to longer-term variations, might help deduce the level to which the deeper ocean is effectively involved by determining the peak phase lag.

The input solar forcing has the expected 11 year cycle and harmonics, but it is dominated by longer periods (>50 years). The GCM response is similar, except that the circa 11 year power is quite muted and not distinguishable from decadal fluctuations inherent in the model itself. As noted by *Hansen et al*. [1988], the ocean model used has an effective mixing below the mixed layer of about 1 $cm^2$ $s^{-1}$ and a climate sensitivity for doubled $CO_2$ of close to 4°C. Analysis shows that for such a combination, the ocean surface response time (time to reach $(1 - e^{-1}$ of equilibrium response) is approximately 125 years [*Hansen et al*., 1985]. Therefore longer-period forcing would be more effective in exciting appreciable responses. However, given that the run with no heat diffusion does not amplify the decadal response, apparently even the mixed layer response time, with an equilibrium time constant of about 10 years, is sufficient. As noted earlier, temperatures over land are somewhat more responsive to the shorter periods.

How relevant are these results to the actual solar-induced climate change during the past 400 years? As noted in the introduction, each aspect of the study may differ from the real world in important ways. The solar forcing change is only an estimate, with little direct information to validate it on these historical timescales. The GCM has a particular climate sensitivity, which while in the range of *IPCC* [1996] estimates, is also not validated; additionally, it has a natural latitudinal response, which may vary from real world conditions [e.g., *Rind*, 1987]. Diffusion below the mixed layer is not the dominant mixing process in the real world, where subduction along isopycnal surfaces produces mixing from near surface to middepth. *Hansen et al*. [1988] configured the diffusion to match observed transient tracer distributions in the ocean, and noted that the response time calculated in this way is not all that different from the response time in coupled atmosphere-ocean models; nevertheless, differences with the real world response time as a function of latitude are likely. Finally, the "no surprise" ocean prohibits solar forcing from exciting changes in ocean heat transports due to thermohaline circulation variations, or

**Table 5.** Relationship Between Precipitation Changes at Various Latitudes and Global Mean Temperature

| Experiment | Precipitation | Linear Regression ($D$precip) = $m$($D$global temp change) + $b$ | Correlation Coefficient |
|---|---|---|---|
| 500 year run | global | $m = 0.07$, $b = -0.01$ | 0.55* |
| | 4°N | $m = 0.03$, $b = -0.09$ | 0.01 |
| | 27°N | $m = 0.002$, $b = 0.01$ | 0.00 |
| | 43°N | $m = 0.09$, $b = 0.007$ | 0.14* |
| | 68°N | $m = 0.12$, $b = 0.01$ | 0.28* |
| No heat diffusion | global | $m = -0.06$, $b = -1.23$ | 0.74* |
| | 4°N | $m = 0.12$, $b = -0.01$ | 0.07 |
| | 27°N | $m = -0.07$, $b = -0.03$ | 0.12† |
| | 43°N | $m = 0.09$, $b = 0.01$ | 0.25* |
| | 68°N | $m = 0.06$, $b = -0.01$ | 0.21* |

*Significant at 1% level.
†Significant at 5% level.

El Niño-type events. While this allows us to clearly differentiate how much solar forcing is doing by itself, in the real world, such feedbacks may well exist.

Various assessments have been made of the spectral decomposition of observed temperature changes during the past 100–150 years [e.g., *Mann and Park*, 1994; *Lau and Weng*, 1995; *Cubasch et al*., 1996]. As in the model, observed peak power occurs in the longer-period modes (40–100 years), which include both the observed trend and the periodicities (e.g., Cubash et al. report power in the 40–60 year range, while Mann and Park found a 90–100 year oscillation). In both the model and the observations there is significant warming in the first 40 years of this century, with subsequent cooling, followed by renewed warming, hence the basic agreement. Note that spectral analysis of the $^{14}C$ record often indicates the presence of >50 year cycles, in particular the 88 year (Gleisberg) cycle, as well as ~200 year periods [e.g., *Damon and Linick*, 1986; *Stuiver et al*., 1991]; these same cycles also appear in varved sediments, implying a climate connection [*Halfman and Johnson*, 1988; *Peterson et al*., 1991; *Anderson*, 1992].

*Mann and Park* [1994] also show a spatial decomposition of the power in different modes. While a full spatial decomposition of the model results is beyond the scope of this paper, the latitudinal distribution can be addressed. The observations show that for this long-period mode, power is greatest at high latitudes, while in the model, it is largest at low latitudes (Figure 4b). This comparison cannot be precise, since *Mann and Park* [1994] had very few observations in the tropics. Nevertheless, it does emphasize that the apparent high-latitude amplification observed in the data does not appear in the model's response to solar forcing. This discrepancy, which we elucidate further in a subsequent paper, supports our overall result that solar irradiance forcing by itself cannot account for all observed global warming in the 20th century.

The observations also show power in the 15–25 year band. Power does exist at these periods in the model, relative to the control run, in both the temperature and the feedbacks (Figures 4b and 5) but not in any statistically significant, stationary sense (Figure 3). *Lau and Weng* [1995] note that it is most prominent from the 1880s to the 1920s, a fact that is not evident in either the input solar forcing or the model's response (Figure 4a). It has long been assumed that power in this range is associated with a 22-year solar forcing (the so-called Hale double sunspot cycle), representative of magnetic oscillations on the Sun. Exotic interactions due to such magnetic fluctuations and their possible consequences, such as variations of cosmic ray flux, with possible impacts on cloud cover [*Svensmark and Friis-Christensen*, 1997], have not been included in these experiments (and therefore could not influence the overall trend either). *Mann and Park* [1994] speculate that a quasi-bidecadal cycle could be a longer-period ENSO effect, which would also not be simulated with the simple ocean model used. As noted above, the mixed layer plus vertical diffusion ocean model would not easily respond to such forcing, given its long time constant. The simulation with no diffusion produced no noticeable increase in power in this band. In experiments with their coupled atmosphere-dynamical ocean model, *Cubasch et al*. [1997] also failed to find significant responses.

Some power exists in observations in the decadal (10–12 year) mode, but in general, it is only weakly evident. The observed effect peaks in the extratropics [*Mann and Park*, 1994] and may be associated with internal ocean or ocean-atmosphere processes in the North Atlantic [*Mehta and Delworth*, 1995; *Halliwell*, 1997], or it may be the direct response to the solar 11 year cycle [e.g., *Lawrence and Ruzmaikin*, 1998; *Steig et al*., 1998]. Again, the response time of the model configuration used here is such as to limit any direct reaction to solar forcing with this short period. Interestingly, decadal power does exist in the model temperature record when there is no direct solar forcing of it (e.g., the Maunder Minimum, Figure 4a), even though no ocean circulation changes are allowed, while *Cubasch et al*. [1997] found no significant stationary decadal power even with ocean circulation changes possible.

*Van Loon and Labitzke* [1988] have found that the 11 year cycle looks much clearer, at least locally and in winter, when partitioned into the appropriate phase of the quasi-biennial oscillation, an effect which has, to some extent, been modeled when including the full stratosphere [*Rind and Balachandran*, 1995]. However, *van Loon and Labitzke* [1994, 1998] also find that even without the QBO influence, an intensified subtropical to midlatitude ridge emerges in phase with the solar cycle. *Haigh* [1996] has emphasized the importance of including ozone variations in any solar cycle/climate impact experiment, and *Shindell et al*. [1998] have found that when using realistic solar forcing with calculated ozone response in a full troposphere/stratosphere model, an amplified ridge does emerge. To the extent that the winds around this feature could alter ocean gyre circulation, it might account for the apparent in-

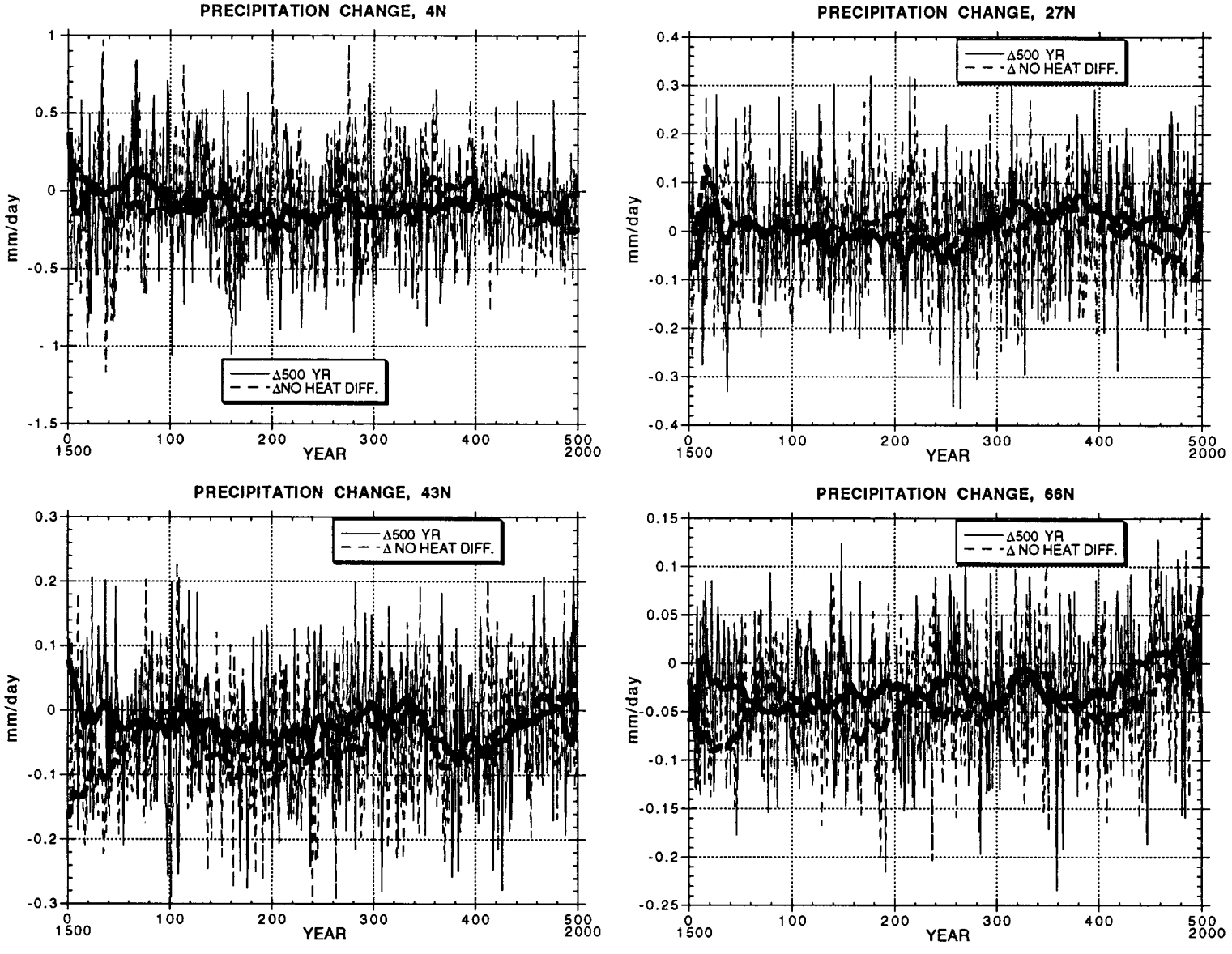


**Figure 12.** Precipitation changes at individual latitudes in experiments 4 and 6.

**Table 6.** Comparison of Solar-Induced, Trace-Gas-induced, and Observed Warming in GISS GCM

| Decade | Solar-Induced Warming | Trace-Gas-Induced Warming | Observed Warming |
|---|---|---|---|
| 1896–1915 minus 1876–1895 | 0 | 0.025 | −0.01 |
| 1916–1935 minus 1876–1895 | 0.015 | 0.128 | 0.110 |
| 1936–1955 minus 1876–1895 | 0.063 | 0.188 | 0.262 |
| 1956–1975 minus 1876–1895 | 0.125 | 0.481 | 0.204 |
| 1976–1995 minus 1876–1895 | 0.194 | 0.707 | 0.451 |

Temperature changes shown are relative to the model results (or observations) for the period 1876–1895. Model values are for global, annual average surface air temperature, while the observations consist of mainly land stations.

phase relationship of the solar cycle and the ocean circulation changes referred to above. To produce such an effect would therefore require a model top above the 10 mbar used here and an inclusion of the photochemical response of ozone.

The model surface temperatures do suggest significant power at 3–4 years (Figure 3), a period found in observations [*Mann and Park*, 1994], and normally considered an ENSO component. Although ENSOs per se do not exist in the mixed layer model, there is a local maximum in surface temperature standard deviation in the tropical eastern Pacific [*Hansen et al*., 1988, Plate 1] (primarily because the cooler temperatures are more easy to increase than the warm temperatures in the western Pacific). The significant peak shown in Figure 3 might have occurred by chance, but if it is a real effect, the response of tropical water vapor to solar forcing may be playing a role in amplifying variability on this timescale.

As expected for this model, the water vapor provides the dominant feedback to the solar forcing. In tandem with the temperature changes, particularly those in the tropics, the water vapor forcing has a predominantly long-period response in phase with the solar forcing. Energy at somewhat shorter periods (greater than about 20 years) also shares these characteristics (Figure 6). The sea ice cover response correlates well with extratropical temperatures, with less energy at the longest periods (Figures 4, 6), and a lower correlation with solar forcing. Total cloud cover has its most energy at the shortest periods (<10 years). Water vapor, most dependent on sea surface temperatures, mimics their long-period response, while cloud cover is more sensitive to interannual relative humidity changes associated with the model's natural variability.

The model results also indicate where precipitation changes are expected. Increases in precipitation occur as a result of solar-induced warming primarily in middle and high latitudes. This is not simply the result of greater warming at these latitudes, for the warming is not that much larger than occurs at other latitudes (see Figure 9; as shown in Table 4, the hemispheric gradient does not actually decrease in all of the runs). At low and subtropical latitudes the change in latitudinal gradient also affects precipitation. A stronger gradient intensifies the Hadley cell and decreases subtropical precipitation, while a weaker gradient decreases tropical precipitation. However, there is little consistent relationship between changes in global temperatures and the low-latitude gradient change (Table 4), or between global temperature and the low-latitude precipitation change (Table 5). As reported by *Karl* [1997], observations also appear to show little consistent precipitation change in the tropics and subtropics over the last century, while there has been noticeable increase in extratropical precipitation as climate has warmed.

A related question is therefore whether it is possible to differentiate the solar from the greenhouse-generated warming on the basis of changes in precipitation and latitudinal gradient. For example, is there greater greenhouse gas-induced warming at 4°N relative to 27°N, compared to the solar forcing (a result that has been suggested, since the lack of cloud cover in the subtropics suggests solar forcing might be more effective there). The model results indicate no such effect, with both slightly greater and slightly reduced low-latitude gradients due to greenhouse forcing relative to solar forcing during the course of the experiment. The only noticeable forcing-specific gradient change which does arise is a greater reduction in the high-latitude gradient with greenhouse forcing, due primarily to the magnitude of the warming being greater in that experiment, hence producing a larger sea ice feedback. As this is a magnitude effect, it has little implications for footprinting the different forcings.

Finally, the question of vertical temperature gradients must be considered. In the model troposphere the temperature gradient decreases, on the global average, as climate warms, with amplified warming in the tropical upper troposphere [e.g., *Hansen et al*., 1988]. As shown by *Hansen et al*. [1984, Figure 4], there is no real difference between solar and $CO_2$ forcing in this respect; therefore any difference in the solar and $CO_2$ forcing runs performed here simply relates to the greater magnitude of the $CO_2$-induced warming over the last century. Nevertheless, the differences are quite small with this degree of warming; for example, the tropospheric static stability (defined here as associated with the temperature difference between 200 mbar and the surface) increases by about 1.5% during the 20th century in the simulation with increased $CO_2$ and less than half of that for the increased solar forcing.

The stratospheric responses might be expected to be quite different. With increased solar forcing, the stratosphere should warm, while with increased $CO_2$, it should cool. These experiments are far from ideal for investigating this issue. In addition to the model's coarse vertical resolution the solar radiation was changed uniformly with wavelength. Presumably, were the solar irradiance change to be associated with variations in faculae and sunspots, the forcing would be significantly larger in the ultraviolet, as it is for solar cycle variations. This would have an impact on ozone production and amplify the stratospheric response. To produce such an effect would also require interactive ozone and a model top position above the 10 mbar location used in these experiments. Thus the temperatures at 10 mbar showed essentially no change with the varying solar forcing, while with increased $CO_2$, cooling of the order of 0.5°C occurred. The effect of solar irradiance spectral variations, and the feedback of resulting ozone and stratospheric changes on the climate system, needs further investigation.

## 6. Conclusions

Using estimated solar forcing variations over the past 400/500 years in the GISS GCM, various GCM experiments were performed. The main conclusions are as follows:

1. Solar irradiance variations account for about 33–50% of the global temperature changes in individual 400 year experiments and 50% of the variance in the standard three-run ensemble.

2. For the ensemble run, the average correlation peaks at 0–20 years.

3. Solar forcing shows a greater correlation with temperature over the ocean due to the generally noisier values over land; response over land peaks at 0–10 years and over the ocean at 0–15 years.

4. Water vapor increases of 2% account for a temperature increase from 1700 to the present of about 0.16°C; water vapor has a 92% correlation with surface air temperature and peaks with zero phase lag.

5. Sea ice decreases of 4% account for a temperature increase of about 0.04°C since 1700; sea ice has a correlation of −0.57 with surface temperature, again highest with zero lag.

6. Cloud cover changes account for a warming of about 0.09°C since 1700, with a high-cloud cover increase and some low-cloud cover decrease; high clouds respond more to the smaller variation temperature changes, with low-cloud effects amplified as the temperature changes increase.

7. The input solar forcing variations, while including the 11 year period and higher harmonics, are dominated by longer periods; so therefore is the model's temperature response, especially in the tropics, with the shorter periods muted by the long response time of the oceans.

8. The water vapor feedback and the tropical temperatures respond with peak power in periods of >50 years and match well the solar forcing at these frequencies; sea ice is more correlated with extratropical temperatures and has less power at longer periods, while cloud cover exhibits primarily high frequency response, as it is less dependent on ocean temperature changes and more on interannual relative humidity variations.

9. Initial conditions influence the model results for 50–80 years, more so when the model must cool, due to its greater sensitivity to cooling (a sea ice effect).

10. Without heat diffusion through the bottom of the ocean mixed layer the model's response is larger, up to a factor of 2; temperature changes over land now peak with a phase lag of 0–5 years and over the ocean at 0–10 years, 5 years faster than with the deep ocean involvement.

11. Solar forcing correlates best with low-latitude temperatures due to the strength of the water vapor feedback; tropical temperatures in turn correlate best with the global response because of their respectively greater area weighting as well as reduced noisiness compared with higher latitudes.

12. Neither the hemispheric nor the low-latitude temperature gradient shows any consistent change with climate change; in the extratropics the gradient decreases as climate warms, which would decrease eddy energy.

13. Global and high-latitude precipitation is positively correlated with global mean temperature changes, but this effect does not occur in the tropics/subtropics, where Hadley cell changes due to altered temperature gradients also affect precipitation; for this magnitude of temperature variation, global precipitation changes are of the order of 1–2%, while individual latitudinal changes of up to 10% occur at times.

14. Solar forcing by itself was not sufficient to produce the rapid warming of the last few decades.

15. The solar-induced warming during the 20th century is about 30% that associated with trace gas warming in this model; if the solar warming is correct, aerosols have produced a negative forcing of some 1.2 W $m^{-2}$, implying an almost equal contribution from direct and indirect tropospheric aerosol effects.

**Acknowledgments.** We thank Ray Bradley and Jonathan Overpeck for the use of their computing facilities during the course of this project and the ARRCC group, in general, for useful comments. N. K. Balachandran helped with the statistical analysis. This work was supported by the joint NOAA and DOE climate detection program, grant NA66GP0426; climate modeling at GISS is supported by the NASA Climate Program Office.

## References

Anderson, R. Y., Possible connection between surface winds, solar activity and the Earth's magnetic field, *Nature*, *358*, 51–53, 1992.

Bloomfield, P., Fourier analysis of time series: An introduction, in *Probability and Mathematical Statistics*, chap. 6, pp. 118–150, John Wiley, New York, 1976.

Bond, G., et al., A pervasive millennial-scale cycle in North Atlantic Holocene and glacial climates, *Science*, *278*, 1257–1266, 1998.

Bradley, R. S., and Jones, P. D., *Climate Since A.D. 1500*, 679 pp., Routledge, New York, 1992.

Cubasch, U., R. Voss, G. C. Hegerl, J. Waszkewitz, and T. Crowley, Simulation of the influence of solar radiation variations on the global climate with an ocean-atmosphere general circulation model, *Clim. Dyn.*, *13*, 757–767, 1997.

Damon, P. E., and T. W. Linick, Geomagnetic-heliomagnetic modulation of atmospheric radiocarbon production, *Radiocarbon*, *28*, 266–278, 1986.

Eddy, J., The Maunder Minimum, *Science*, *192*, 1189–1202, 1976.

Frohlich, C., and J. Lean, The sun's total irradiance: Cycles, trends and climate change uncertainties since 1976, *Geophys. Res. Lett.*, in press, 1998.

Haigh, J. D., The impact of solar variability on climate, *Science*, *272*, 981–984, 1996.

Halfman, J. D., and T. C. Johnson, High resolution record of cyclic climatic change during the past 4 ka from Lake Turkana, Kenya, *Geology*, *16*, 496–500, 1988.

Halliwell, G. R., Jr., Decadal and multidecadal North Atlantic SST anomalies driven by standing and propagating basin-scale atmospheric anomalies, *J. Clim.*, *10*, 2405–2411, 1997.

Hansen, J. E., G. Russell, D. Rind, P. Stone, A. Lacis, S. Lebedeff, R. Ruedy, and L. Travis, Efficient three-dimensional global models for climate studies: Models I and II, *Mon. Weather Rev.*, *111*, 609–662, 1983.

Hansen, J., A. Lacis, D. Rind, G. Russell, P. Stone, I. Fung, R. Ruedy, and J. Lerner, Climate sensitivity: Analysis of feedback mechanisms, in *Climate Processes and Climate Sensitivity*, *Geophys. Monogr.*, vol. 29, edited by J. Hansen and T. Takahashi, pp. 130–163, AGU, Washington, D. C., 1984.

Hansen, J., G. Russell, A. Lacis, I. Fung, D. Rind, and P. Stone, Climate response times: Dependence on climate sensitivity and ocean mixing, *Science*, *229*, 857–859, 1985.

Hansen, J., I. Fung, A. Lacis, D. Rind, S. Lebedeff, R. Ruedy, and G. Russell, Global climate changes as forecast by Goddard Institute for Space Studies three-dimensional model, *J. Geophys. Res.*, *93*, 9341–9364, 1988.

Horne, J., and S. Baliunas, A prescription for period analysis of unevenly sampled time series, *Astrophys. J.*, *302*, 757–763, 1986.

Hoyt, D. V., and K. H. Schatten, A discussion of plausible solar irradiance variations, 1700–1992, *J. Geophys. Res.*, *98*, 18,895–18,906, 1993.

Hoyt, D. V., K. H. Schatten, and E. Nesmes-Ribes, The one hundredth year of Rudolf Wolf's death: Do we have the correct reconstruction of solar activity?, *Geophys. Res. Lett.*, *21*, 2067–2070, 1994.

Intergovernmental Panel on Climate Change (IPCC), *Climate Change 1995*, edited by J. T. Houghton, L. G. Meira Filho, B. A. Callander, N. Harris, A. Kattenberg, and K. Maskell, 572 pp., Cambridge Univ. Press, New York, 1995.

Karl, T. R., Observed changes in precipitation intensity: Evidence for an enhanced hydrologic cycle?, *Eos Trans. AGU*, *78*(46), Fall Meet. Suppl., F113, 1997.

Kelly, P. M., and T. M. L. Wigley, Solar cycle length, greenhouse forcing and global climate, *Nature*, *360*, 328–330, 1992.

Lau, K.-M., and H. Weng, Climate signal detection using wavelet transform: How to make a time series sing, *Bull. Am. Meteorol. Soc.*, *76*, 2391–2402, 1995.

Lawrence, J. K., and A. A. Ruzmaikin, Transient solar influence on terrestrial temperature fluctuations, *Geophys. Res. Lett.*, *25*, 159–162, 1998.

Lean, J., A. Skumanich, and O. R. White, Estimating the sun's radiative output during the Maunder Minimum, *Geophys. Res. Lett*., *19*, 1591–1594, 1992.

Lean, J., J. Beer, and R. Bradley, Reconstruction of solar irradiance since 1610: Implications for climate change, *Geophys. Res. Lett*., *22*, 3195–3198, 1995.

Mann, M. E., and J. Park, Global-scale modes of surface temperature variability on interannual to century timescales, *J. Geophys. Res*., *99*, 25,819–25,833, 1994.

Mann, M. E., R. S. Bradley, and M. K. Hughes, Global-scale temperature patterns and climate forcing over the past six centuries, *Nature*, *392*, 779–787, 1998.

Mehta, V. M., and T. Delworth, Decadal variability in the tropical Atlantic Ocean surface temperature in shipboard measurements and a global ocean-atmosphere model, *J. Clim*., *8*, 172–190, 1995.

Peterson, L. C., J. T. Overpeck, N. Kipp, and J. Imbrie, A high resolution Late-Quaternary upwelling record from the anoxic Cariaco Basin, Venezuela, *Paleoceanography*, *6*, 99–119, 1991.

Prabhakara, C., R. Iacovazzi, Jr., J.-M. Yoo, and G. Dalu, Global warming deduced from MSU, *Geophys. Res. Lett*., *25*, 1927–1930, 1998.

Reid, G. C., Solar forcing of global climate chance since the mid-17th century, *Clim. Change*, *37*, 391–405, 1997.

Rind, D., The dynamics of warm and cold climates, *J. Atmos. Sci*., *43*, 3–24, 1986.

Rind, D., The doubled $CO_2$ climate: Impact of the sea surface temperature gradient, *J. Atmos. Sci*., *44*, 3235–3268, 1987.

Rind, D., Latitudinal temperature gradients and climate change, *J. Geophys. Res*., *103*, 5943–5971, 1998.

Rind, D., and N. K. Balachandran, Modeling the effects of UV variability and the QBO on the troposphere-stratosphere system, II, The troposphere, *J. Clim*., *8*, 2080–2095, 1995.

Rind, D., and J. Overpeck, Hypothesized causes of decade-to-century-scale climate variability: Climate model results, *Quat. Sci. Rev*., *12*, 357–374, 1994.

Rind, D., R. Healy, C. Parkinson, and D. Martinson, The role of sea ice in $2 \times CO_2$, Climate model sensitivity, 1, The total influence of sea ice thickness and extent, *J. Clim*., *8*, 449–463, 1995.

Schlesinger, M. E., and N. Ramankutty, Implications for global warming of intercycle solar irradiance variations, *Nature*, *360*, 330–333, 1992.

Steig, E. J., D. L. Morse, E. D. Waddington, and P. J. Polissar, Using the sunspot cycle to date ice cores, *Geophys. Res. Lett*., *25*, 163–166, 1998.

Stuiver, M., T. F. Braziunas, B. Becker, and B. Kromer, Climatic, solar, oceanic and geomagnetic influences on late-Glacial and Holocene atmospheric $^{14}C/^{12}C$ change, *Q. Res*., *35*, 1–24, 1991.

Svensmark, H., and E. Friis-Christensen, Variation of cosmic ray flux and global cloud coverage—A missing link in solar-climate relationships, *J. Atmos. Solar Terr. Phys*., *59*, 1225–1232, 1977.

van Loon, H., and K. Labitzke, Association between the 11-yr solar cycle, the QBO and the atmosphere, II, Surface and 700 mb in the Northern Hemisphere in winter, *J. Clim*., *1*, 905–920, 1988.

van Loon, H., and K. Labitzke, The 10–12 year atmospheric oscillation, *Meteorol. Z*., *3*, 259–266, 1994.

van Loon, H., and K. Labitzke, The global range of the stratospheric decadal wave, I, Its association with the sunspot cycle in summer and in the annual mean, and with the troposphere, *J. Clim*., *11*, 1529–1537, 1998.

White, W. B., J. Lean, D. R. Cayan, and M. D. Dettinger, Response of global upper ocean temperature to changing solar irradiance, *J. Geophys. Res*., *102*, 3255–3266, 1997.

R. Healy, Center for Climate Systems Research, Columbia University, New York, NY 10027.

J. Lean, E. O. Hulbert Center for Space Research, Naval Research Laboratory, Washington, D. C. 20375.

D. Rind, NASA Goddard Space Flight Center, Institute for Space Studies, New York, NY 10025. (e-mail: drind@giss.nasa.gov)

(Received May 6, 1998; revised August 21, 1998;
accepted August 27, 1998.)